


Bone-Induced Chondroinduction in Sheep Jamshidi Biopsy Defects with and without Treatment by Subchondral Chitosan-Blood Implant: 1-Day, 3-Week, and 3-Month Repair

Cartilage
4(2) 131–143
© The Author(s) 2012
Reprints and permission:
sagepub.com/journalsPermissions.nav
DOI: 10.1177/1947603512463227
http://cart.sagepub.com


Angela D. Bell, MSc¹, Viorica Lascau-Coman, MSc², Jun Sun, MD, MSc³, Gaoping Chen, MD², Mark W. Lowerison, MSc¹, Mark B. Hurtig, DVM, MVSc¹, and Caroline D. Hoemann, PhD^{2,4}

Abstract

Objective: Delivery of chitosan to subchondral bone is a novel approach for augmented marrow stimulation. We evaluated the effect of 3 presolidified chitosan-blood implant formulations on osteochondral repair progression compared with untreated defects. **Design:** In $N = 5$ adult sheep, six 2-mm diameter Jamshidi biopsy holes were created bilaterally in the medial femoral condyle and treated with presolidified chitosan-blood implant with fluorescent chitosan tracer (10 kDa, 40 kDa, or 150k Da chitosan, left knee) or left to bleed (untreated, right knee). Implant residency and osteochondral repair were assessed at 1 day ($N = 1$), 3 weeks ($N = 2$), or 3 months ($N = 2$) postoperative using fluorescence microscopy, histomorphometry, stereology, and micro-computed tomography. **Results:** Chitosan implants were retained in 89% of treated Jamshidi holes up to 3 weeks postoperative. At 3 weeks, biopsy sites were variably covered by cartilage flow, and most bone holes contained cartilage flow fragments and heterogeneous granulation tissues with sparse leukocytes, stromal cells, and occasional adipocytes (volume density 1% to 3%). After 3 months of repair, most Jamshidi bone holes were deeper, remodeling at the edges, filled with angiogenic granulation tissue, and lined with variably sized chondrogenic foci fused to bone trabeculae or actively repairing bone plate. The 150-kDa chitosan implant elicited more subchondral cartilage formation compared with 40-kDa chitosan-treated and control defects ($P < 0.05$, $N = 4$). Treated defects contained more mineralized repair tissue than control defects at 3 months ($P < 0.05$, $N = 12$). **Conclusion:** Bone plate-induced chondroinduction is an articular cartilage repair mechanism. Jamshidi biopsy repair takes longer than 3 months and can be influenced by subchondral chitosan-blood implant.

Keywords

chitosan, osteochondral repair, micro-computed tomography, large animal model, marrow stimulation, bone plate, chondrogenesis, coagulation, Jamshidi

Introduction

Microfracture is used to treat full-thickness cartilage lesions,¹ however, improvements to the technique are needed because repair is often incomplete and composed of a combination of fibrous connective tissue and fibrocartilage rather than hyaline cartilage.^{2–4} An *in situ* solidifying chitosan-blood clot implant was reported to improve the hyaline quality of repair tissue compared with microfracture or drilling alone.^{5,6} Chitosan is a biodegradable polysaccharide,⁷ which attracts neutrophils and alternatively activated macrophages, which degrade the biomaterial *in situ*.^{8,9} In rabbit cartilage repair models, a chitosan-induced transient accumulation of innate immune cells was associated with

enhanced subchondral angiogenesis, woven bone repair, osteoclast-mediated bone remodeling, and delayed and displaced formation of chondrogenic foci to the surface of

¹Department of Clinical Studies, University of Guelph, Guelph, Ontario, Canada

²Department of Chemical Engineering, École Polytechnique, Montreal, Quebec, Canada

³BioSyntech/Piramal Healthcare Canada, Montreal, Quebec, Canada

⁴Institute of Biomedical Engineering, École Polytechnique, Montreal, Quebec, Canada

Corresponding Author:

Caroline D. Hoemann, Department of Chemical Engineering, École Polytechnique, Montreal, Quebec, H3C 3A7, Canada
Email: caroline.hoemann@polymtl.ca

the bone marrow stimulation holes.^{5,8-13} In clinical practice, the *in situ* solidifying chitosan-blood implant (BST-CarGel, Piramal Healthcare, Laval, Quebec, Canada) is used to flood the surface of a chondral defect in the knee while the lesion is maintained in a horizontal orientation.⁶ In this study, we designed a presolidified implant containing chitosan microparticles dispersed in a whole blood clot to improve handling and to allow chitosan delivery to bleeding holes created in treated articular surfaces in all orientations. We hypothesized that chitosan implanted into the subchondral bone of large animals in this manner could be retained and have a therapeutic effect on osteochondral repair similar to that reported for chitosan deposited above the subchondral bone.

The importance of restoring the subchondral bone plate has been recognized as an integral component of cartilage repair.¹⁴ Therefore, the aim of cartilage repair should be restoration of the depth-dependent architecture of the articular surface as a functional osteochondral weight-bearing unit.¹⁴ Detrimental subchondral bone changes can occur with the use of marrow stimulation techniques. Up to 30% of patients treated with microfracture develop subchondral cysts, subchondral bone plate thickening, and overgrowth of bone within the lesion.¹⁵ Subchondral cysts, thickening, and osteophyte formation have unfortunate effects on the mechanical environment of the cartilage. These changes may cause abnormal contact pressures and contribute to the progression of osteoarthritis.¹⁵⁻¹⁷ Therefore, augmented marrow stimulation therapy should specifically aim to stimulate damaged subchondral bone repair while suppressing abnormal bone reactions.

The purpose of this study was to explore the use of novel presolidified chitosan formulations as therapeutic subchondral implants for bone marrow-derived cartilage repair in a large animal model. Timely clearance of a subchondral chitosan implant could require the use of a lower molecular mass chitosan formulation. Therefore, we tested 3 distinct molecular weight chitosan formulations in this model. A Jamshidi needle (11G) generates a cylindrical, ~2.3-mm diameter bone hole (C. D. Hoemann *et al.*, unpublished data) similar in shape to a drill hole and is better suited to receive a cylindrical-shaped implant compared with a tapered microfracture hole that is 1.2 to 2.0 mm wide at the top (depending on the awl used and depth of perforation; C. D. Hoemann *et al.*, unpublished data). Furthermore, a Jamshidi biopsy recovered from the lesion removes an osteochondral core that could be potentially analyzed for diagnostic purposes. Given these reasons, in this study Jamshidi bone biopsy needles were used as an alternative marrow stimulation approach.

Methods

Sheep Osteochondral Model

Housing, care, and the study protocol were approved by institutional animal care committees according to Canadian

Council for Animal Care guidelines. Five skeletally mature Arcott cross female sheep from specific pathogen-free herds (2-4 years old, 65-93 kg) received prophylactic antibiotics (20,000 IU/kg penicillin and 2.2 mg/kg gentamicin) and nonsteroidal anti-inflammatory pain medication (1.1 mg/kg flunixin intravenous, 100 µg transdermal fentanyl patch) during surgery and were anesthetized with intravenous ketamine and diazepam and maintained on isoflurane gas. Using aseptic technique, a medial infrapatellar arthrotomy was used to create 6 holes, 2.5- to 8.5-mm deep, with a 11G Jamshidi biopsy needle (2-mm inner diameter, Cardinal Health, Dublin, OH) and mallet in the weight-bearing area of the medial femoral condyle (MFC) of each leg. In the right MFC, the Jamshidi holes were allowed to bleed as controls while each hole in the left MFC was treated with a presolidified chitosan-blood implant (see below). Osteochondral biopsies were retrieved and the bone length measured with a ruler and subsequently verified by histomorphometry with a dissection microscope with digital camera and calibrated software (Northern Eclipse, Empix, Mississauga, Ontario, Canada). The arthrotomy site was closed in 3 separate layers with absorbable suture material and skin staples. No knee joint immobilization was used because this is contraindicated after joint surgery and is not the standard of care for patients. All animals received postoperative nonsteroidal anti-inflammatory pain medication (1.1 mg/kg flunixin) for 3 days and as required for up to 2 weeks. Sheep were euthanized after 1 day ($N = 1$), 21 days ($N = 2$), and 93 days ($N = 2$). During necropsy, all joints were humidified with lactated Ringer's solution. Defect sites were photographed with a digital camera. The general macroscopic appearance (smooth to rough, 0-2), presence of osteophytes (none to >50% of the condyle rim, 0-3) and the International Cartilage Repair Society visual score (no lesion to lesion into the bone, 0-4),^{18,19} and repair tissue characteristics were documented. The macroscopic scoring system ranges from 0 to 9 where 0 represents normal cartilage.

Generation of Chitosan-NaCl/blood implants

Chitosan-free base powders were provided by BioSyntech, Laval, Quebec, Canada (now Piramal Healthcare Canada) with degree of deacetylation between 80.2% and 81.9% and number-average molecular mass (M_n) 226 to 241 kDa (**Table 1**). All chitosans prior to depolymerization and solution preparation had initial medical-grade purity: ≤ 5 ppm heavy metals, $\leq 0.20\%$ ash, < 500 EU/g, $< 0.20\%$ protein. Chitosan was depolymerized in nitrous acid to a target molecular mass of ~40 or ~10 kDa.²⁰ Formulations were prepared in sterile cryovials containing 3, sterile 0.39 g stainless steel mixing beads, 200 µL autoclave-sterile 2% w/v chitosan-HCl (150 kDa, 40 kDa, or 10 kDa), 25 µL of filter-sterile 5 mg/mL rhodamine isothiocyanate (RITC)-chitosan-HCl with matching molecular mass (**Table 1**), synthesized according to Ma *et al.*²¹ at 1% mol/mol RITC/

Table 1. Chitosan Structural Characterization for the 3 Chitosan Solutions

Chitosan Solution	Chitosan Powder Lot Number, Lot Number after Depolymerization	DDA (%)	M _n (kDa)	PDI
10K				
10K01	CH0100609A, 80B10-D-3835-010	81.9	12.7 ^a	1.87 ^a
RITC-10K	PCCH00057, 57-10-2	80.0	10.3 ^b	2.21 ^b
40K				
40K	CH10075, 80B40-B40-D-3634-003	80.2	25.3 ^a	1.24 ^a
RITC-40K	CH10075, 80B40-B40-D-3634-003	80.2	37.7 ^b	1.28 ^b
150K				
80M4	CH0100708A	81.8	107.4 ^a	1.16 ^a
RITC-80M3	CH0100708A	81.8	241.2 ^b	1.14 ^b

Abbreviations: DDA = degree of deacetylation; M_n = number average molecular weight; RITC = rhodamine isothiocyanate; PDI = polydispersity index (M_w/M_n).

^aValues analyzed after autoclave sterilization.

^bValues prior to RITC derivatization, which increases DDA by ~1% with no significant change in M_n after filter sterilization.²¹

chitosan, and 50 μ L filter-sterile 750 mM NaCl. The M_n and polydispersity index (PDI, M_w/M_n) of chitosans before and after autoclave were determined by size exclusion chromatography in sodium acetate mobile phase followed by GPC (gel permeation chromatography) triple detection light scattering as described.²¹ After Jamshidi biopsy defect creation, 5 mL of fresh autologous sheep blood was drawn from the jugular vein, and 1.5 mL sterile whole blood was distributed to 3 cryovials containing 150-, 40-, or 10-kDa chitosan formulation. Each vial was shaken for 10 seconds, drawn aseptically into sterile glass tubes with a 2-mm inner diameter, solidified in a sterile tray for 20 to 30 minutes at 37 °C, extruded into a sterile plastic petri dish, and trimmed to approximately 3 mm with a scalpel prior to implanting into 2 Jamshidi holes per condyle per formulation (holes 1 and 4—150-kDa implant; holes 2 and 5—40-kDa implant; holes 3 and 6—10-kDa implant, see **Fig. 1A**).

Micro-computed Tomography (μ CT) Analysis

Intact knee joints were scanned at a resolution of 45 μ m (GE Locus eXplore, Milwaukee, WI) to observe global bone characteristics, and the condyles removed with a band saw, fixed in 4% paraformaldehyde/100 mM cacodylate pH 7.4, and rescanned at a resolution of 27 μ m for detailed analysis of each hole. Scans were calibrated against water, air, and a hydroxyapatite-containing phantom (SB3, 1.82 g/cm³, Gammex, Middleton, WI) and reconstructed using GE Medical Systems eXplore Reconstruction Utility. A standardized morphometric analysis of hole depth, and cross-sectional area (at 6 distinct positions in each hole) was undertaken in GE Medical Systems eXplore MicroView version 2.2 using data sets repositioned in a coronal view for each hole. Hole diameter (D) was calculated based on the formula: $D = 2 \times \sqrt{(\text{cross-sectional area}) / 3.14}$. A novel radial analysis method of bone repair in subchondral bone defects was developed. To generate the quantitative measures, the central axis of each Jamshidi hole was

established in the trabecular bone region below the subchondral bone plate and 1 to 2 mm above the bottom of the hole. Linear measures were then performed within each image slice radially in 4 directions and extending 1.5 mm from the central axis to include the hole, the original sidewall of the hole, and several millimeters beyond the initial sidewall of the hole. Approximately 140 slices (at 27- μ m increments) through a 3-mm deep region were analyzed in each hole from the center across 4 planes. ImageJ (version 1.42) was then used to create text files that contained the X , Y , and Z coordinates of each voxel in the μ CT images along with their corresponding gray scale intensity value. A virtual ashing procedure from GE (MicroView) was used to turn the intensities to mineral content. Software was developed in Python (version 3.1.1) and Cran-R (www.r-project.org) to determine radial gradients in bone mineral density and bone volume fraction from the central axis of the hole to beyond the repair tissue-bone interface using the text files created in ImageJ. The bone threshold was calculated using Ng's method.²² The average bone mineral density (g/cm³) and bone volume fraction (%) radiating from the center of the hole were obtained for individual Jamshidi holes for 1-day repair ($N = 12$ treated and control holes), and holes treated with implant versus controls for 3-week repair ($N = 12$) and 3-month repair ($N = 12$).

Epifluorescence, Histostaining, Immunohistochemistry, and Histomorphometric Analysis

Condyle articular surfaces were placed face-down in buffered saline in a petri dish, and fluorescent implant residency documented using a Zeiss inverted epifluorescent microscope with a 1.25 \times objective and Northern Eclipse (Mississauga, Ontario, Canada) equipped with a digital camera to acquire an image of each Jamshidi hole using the same exposure time. Untreated condyles showed no fluorescence. Fixed condyles were cut transversely into two halves with an isomet low-speed diamond saw. The

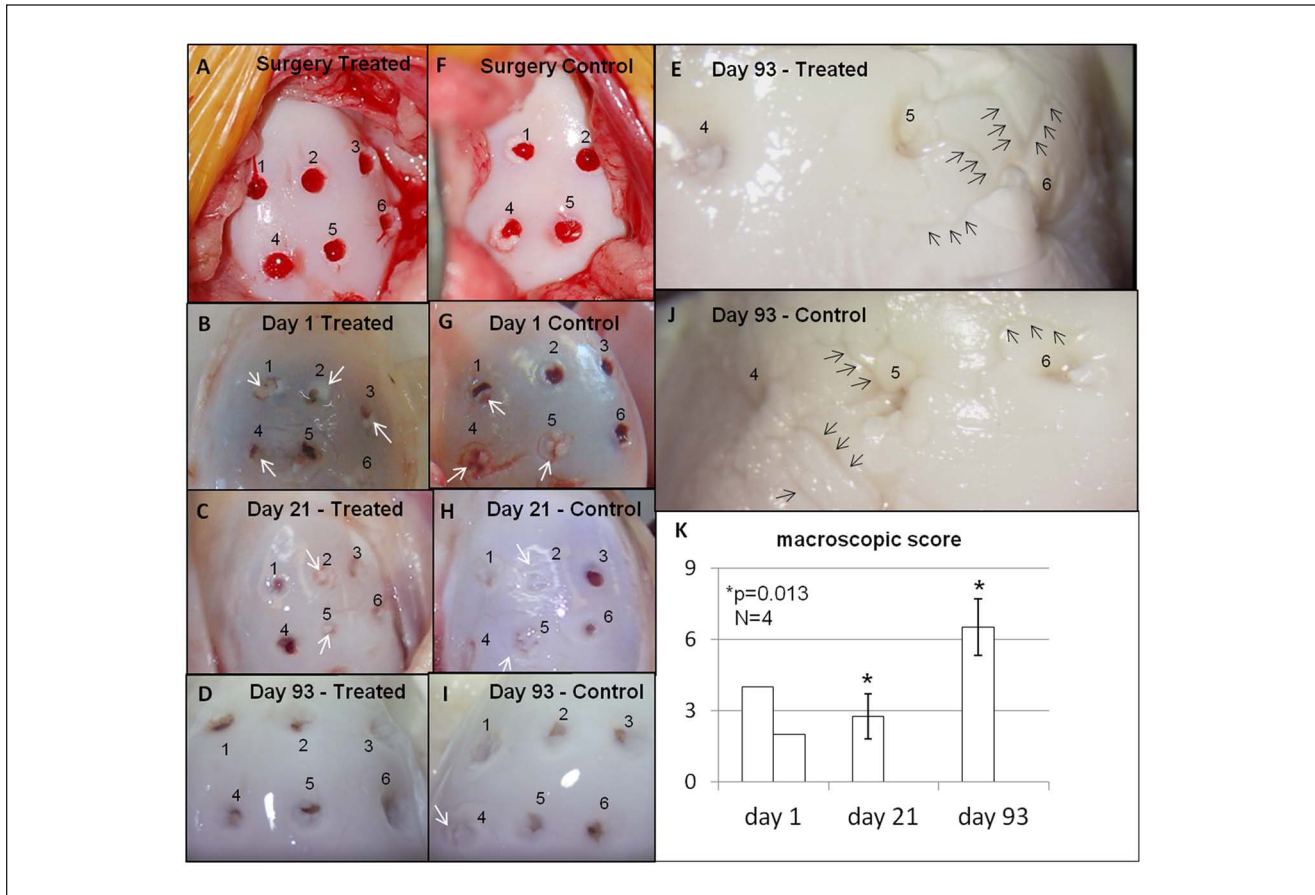


Figure 1. Macroscopic appearance (**A-J**) and macroscopic scores (**K**) of treated (**A-E**) and contralateral control medial femoral condyles (**F-J**) were similar at surgery (**A, F**), after 1 day (**B, G**), 21 days (**C, H**), and 93 days (**D-E, I-J**) postoperative. The overall macroscopic score of condyles deteriorated significantly between 21 and 93 days postoperative ($P = 0.013$, $N = 4$, day 21 and 93, mean \pm SD) mainly because of osteophytes. Overall scores ranged from 2 to 8, in which a score of 0 is normal cartilage, and was determined from general articular cartilage appearance (smooth-rough, 0-2), osteophytes (none to >50% of condyle margin, 0-3) and International Cartilage Repair Society (ICRS) lesion grade (no lesion to exposed bone, 0-4). Black arrows in (**E** and **J**) point to cartilage fissuring whereas the white arrows (**B, C, G, and H**) point to macroscopically visible articular cartilage flow covering the Jamshidi holes.

proximal half with 3 Jamshidi holes was decalcified with 10% ethylenediaminetetraacetic acid (EDTA)/0.1% paraformaldehyde with a Micromed T/T histology microwave (Milestone, Shelton, CT) at 37 °C and embedded in OCT for cryosectioning using the CryoJane tape-transfer system (Instrumedics, St Louis, MO). The distal half containing three Jamshidi holes was immersed in alcohol, infiltrated, and embedded in methylmethacrylate (MMA). Serial sections were collected through the 3 holes as close to the middle of the holes as possible. Sections were stained with Safranin O/Fast Green/iron hematoxylin, and cryosections were also stained with Gomori Trichrome (cryosections), and MMA sections with Goldner's Trichrome and von Kossa-toluidine blue. Cryosections and deplastified MMA sections were also immunostained for collagen type II using mouse monoclonal II6B3 (Developmental Studies Hybridoma Bank, Iowa City, IA), collagen type I using

mouse monoclonal I-8H5 (Cedarlane, Mississauga, Ontario, Canada), biotinylated secondary, and the ABC-AP red substrate detection, using pronase and hyaluronidase pretreatment, and a 30-minute incubation in 65 °C Tris pH 10.0 as previously described to unmask epitopes.⁵ Unbiased stereology was carried out on 40 \times magnification images taken in the center of each hole at 0, 0.5, 1.0, 1.5, and 2.5 mm depth below the tidemark, and excluding bone, with fewer fields taken in shallower holes. A grid with 8 μ m \times 8 μ m squares and 588 intersections (i.e., points, P_{total}) was randomly superimposed on each image and selected cell types (white blood cells with intact nuclei, stromal cells, chondrocytes (from cartilage flow) and adipocytes) were counted if they touched any of the grid intersections (P_{cells}).⁸ The volume density of each cell type and total cells in the tissue was calculated with the formula: $V_v = \sum P_{\text{cells}} / \sum P_{\text{total}}$ (units: m^0). V_v was determined for $N = 1$ to 3 sections

Table 2. Jamshidi Bone Core Length at Surgery and Micro-Computed Tomography (μ CT) Bone Hole Dimensions at Necropsy (Mean \pm SD)

Group	No. of Holes Analyzed	Bone Core Length (mm)	μ CT Hole Depth (mm)	Change ^a (mm)	μ CT Hole Diameter (mm)	Change ^b (mm)
All day 1	10	5.7 \pm 1.7	5.7 \pm 1.3	0.0	2.2 \pm 0.7	—
Day 21 (treated)	10	4.3 \pm 1.9	4.0 \pm 1.7	-0.3	2.2 \pm 1.1	0.0
Day 21 (control)	12	5.4 \pm 1.2	5.3 \pm 1.6	-0.1	2.2 \pm 0.8	0.0
Day 93 (treated)	11	3.9 \pm 1.2	5.3 \pm 1.6	1.4	2.3 \pm 1.5	0.1
Day 93 (control)	12	3.8 \pm 1.2	4.9 \pm 1.1	1.1	2.2 \pm 1.1	0.0

^a μ CT depth versus bone core length.

^b μ CT hole diameter: 3 weeks and 3 months versus day 1.

through each hole, and 1 to 4 different levels, averaged to give 1 Vv value per hole, and submitted to statistical analysis with $N = 12$ (treated) and $N = 12$ (control). Structural integrity of the repair tissue and surrounding cartilage was scored on blinded Safranin O–stained sections, on a scale of 0 to 3 where 0 is no cartilage covering the hole, 1 is fissured or degraded cartilage, 2 is covered with irregular cartilage, and 3 is intact cartilage. Volume of soft repair tissue above and below the projected tidemark and percentage Safranin O positive stained repair tissue below the tidemark either along the walls of the hole or at the bottom of the hole was determined using calibrated Northern Eclipse histomorphometric software (Empix Imaging, Mississauga, Ontario, Canada) with images acquired with an Olympus BX60 microscope and CCD camera. Cartilage flow (articular cartilage originally surrounding the holes that is pushed below the tidemark) was quantified by thresholding collagen type II positive stained tissue that has flowed from the surrounding articular cartilage to below the tidemark in the hole and then normalizing to the total area of the repair tissue below the tidemark. “Mature” chondrogenic foci were large and contained hypertrophic chondrocytes, whereas foci detected in only one section level with no hypertrophic chondrocytes were considered “small” or “nascent.”¹²

Statistical Analyses

Analysis of variance was used to test for significant differences in histomorphometric analyses between sample groups ($N = 4$ for each chitosan treatment and contralateral control) and Student’s equal variance 2-tailed t tests with the Bonferroni–Holm correction were computed for parameters that showed significance with analysis of variance. The general linear model (Statistica, V6.2, StatSoft, Tulsa, OK) was used to test the effect of implant treatment on Vv for different cell types at 3 weeks postoperative ($N = 12$ treated vs. control holes), as well as the effect of implant treatment on bone volume fraction at 3 months postoperative with average bone volume fraction values at 3 systematic

locations from the central axis as categorical predictors (0.5 mm, 0.75 mm and 1.0 mm, $N = 12$ treated vs. $N = 12$ control defects). Linear regression analysis analyzed percentage Safranin O–stained subchondral repair cartilage of all defects at 3 months *versus* average hole cross-sectional area ($N = 24$), hole depth at surgery, or hole depth at 3 months; $P < 0.05$ was considered significant.

Results

Jamshidi Defect Macroscopic Appearance and Implant Residency

Six Jamshidi biopsy holes were created in 2 rows in each medial femoral condyle (**Fig. 1A** and **B**). It was technically difficult to core the highly dense sheep bone to a precise target depth of 4 mm, and the initial hole depth ranged from 2 to 6.5 mm (see average bone core length, **Table 2**). Presolidified chitosan–blood implants kept a cylindrical shape after extrusion from the glass tubes used to induce implant coagulation (**Fig. 2A** and **B**). The implants were elastic, could be trimmed with a scalpel, and self-inserted into the Jamshidi holes by passive capillary action (**Fig. 1A**). Fluorescent implant was detected macroscopically in 89% of defects (16 out of 18) at 1 and 21 days, with diminishing fluorescence over time, suggesting chitosan clearance (**Fig. 2C** to **H**). At 3 weeks postoperative, residual chitosan particles were mainly detected at the edges or base of the defect (**Fig. 2I** and **J**).

A blue hue under the cartilage developed in both day 1 condyles, consistent with biopsy-induced subchondral bleeding (**Fig. 1B** and **G**). All biopsy holes were still macroscopically visible at 3 weeks and 3 months postoperative (**Fig. 1C–E**, **H–J**). Articular cartilage flow covered some holes even after 1 day (white arrows, **Fig. 1**). Fissuring or marbling of the articular cartilage developed around the Jamshidi holes in 3 out of 10 condyles (2 treated and 1 control) at day 1 and day 93 (black arrows, **Fig. 1E** and **J**). Global macroscopic scores of all condyles worsened over the course of the repair period ($P = 0.013$, **Fig. 1K**), mainly

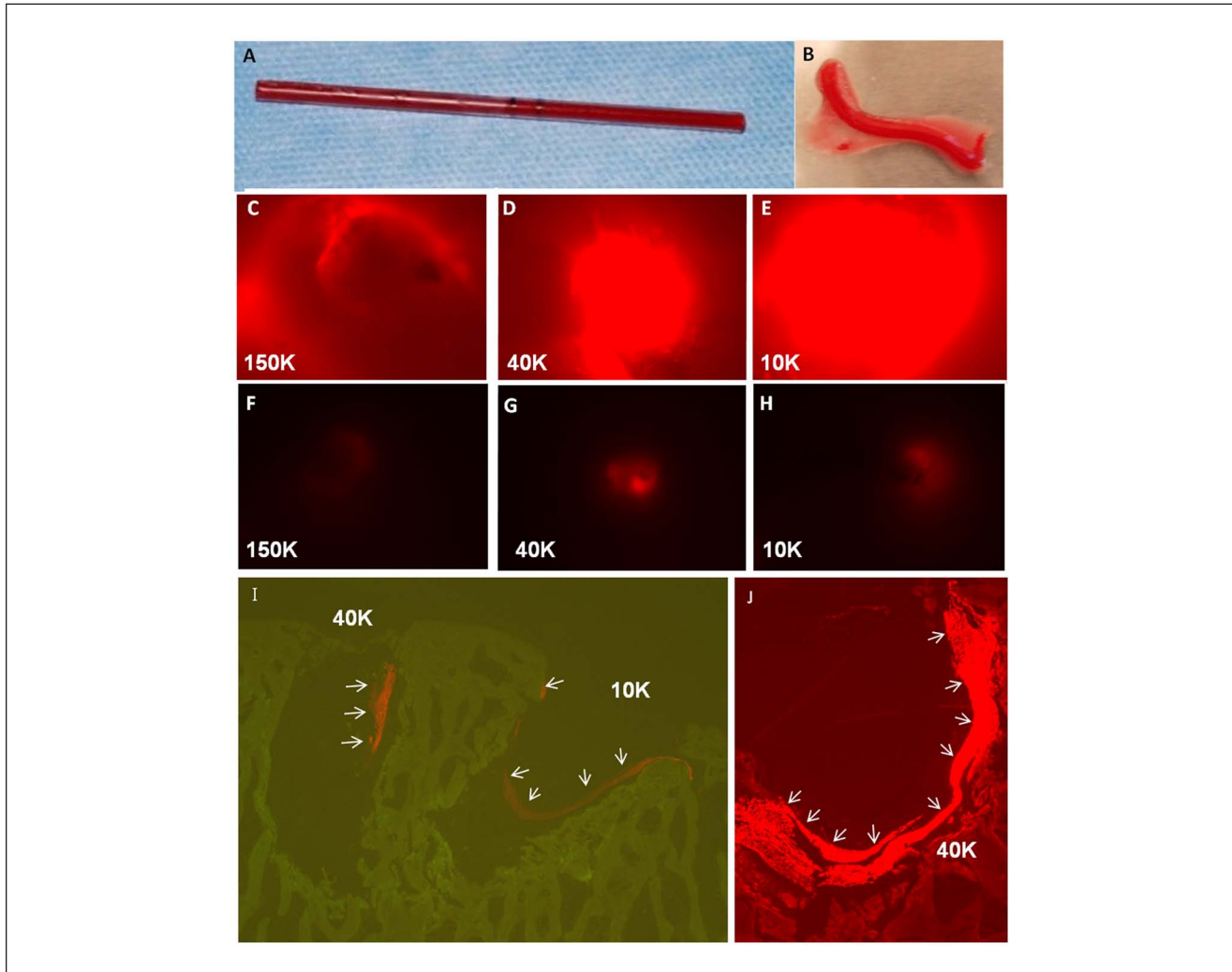


Figure 2. Implant generation and residency. Chitosan-blood implants were solidified in glass tubes (**A**) and extruded into sterile dishes (**B**) where they were trimmed with a scalpel before implanting. Day-1 and 3-week defects were treated with implants containing rhodamine isothiocyanate (RITC)-chitosan tracer to visualize implant residency in treated holes after 1 day (**C-E**) and 3 weeks (**F-H**) *in vivo*. Control holes showed no fluorescence (data not shown). At 3 weeks postoperative, residual implant was mainly detected along the perimeter of the defect: (**I**) red fluorescent RITC-chitosan tracer and green autofluorescent bone and (**J**) bright red RITC-chitosan and red autofluorescent bone, images from unstained, nondecalcified methylmethacrylate (MMA) sections.

because of development of osteophytes. At necropsy, joint surfaces other than the medial condyle were generally smooth and the menisci undamaged.

Cell Recruitment and Chondroinduction

At day 1 postoperative all Jamshidi holes were filled with blood clot that in some defects also contained articular cartilage fragments or marrow-derived adipose tissue fragments (**Fig. 3A to C**). Treated defects additionally contained chitosan particles (**Fig. 2C to E**). At 3 weeks postoperative, articular cartilage flow covered many defects and cartilage fragments depleted of glycosaminoglycan were pushed into many holes from adjacent cartilage (black arrowheads,

Fig. 3F and G). Significantly more chondrocytes in cartilage flow (CCF) were detected inside of control versus treated holes ($P = 0.013$, **Fig. 4A**). Cartilage flow may have resulted from a combination of immediate weight bearing after surgery and because of cartilage swelling following disruption of the collagen network at the cored cartilage edge. Jamshidi holes at 3 weeks contained a mixed hypocellular tissue with low volume density (Vv) of leukocytes, stromal cells, and adipocytes (**Fig. 4A and B**). Only one untreated Jamshidi hole contained angiogenic blood vessels and highly abundant stromal cells (**Fig. 3H**, right hole).

At 3 months postoperative, Jamshidi defects were partly covered by marrow-derived repair tissue, and partly by cartilage flow that often extended below the tidemark (white

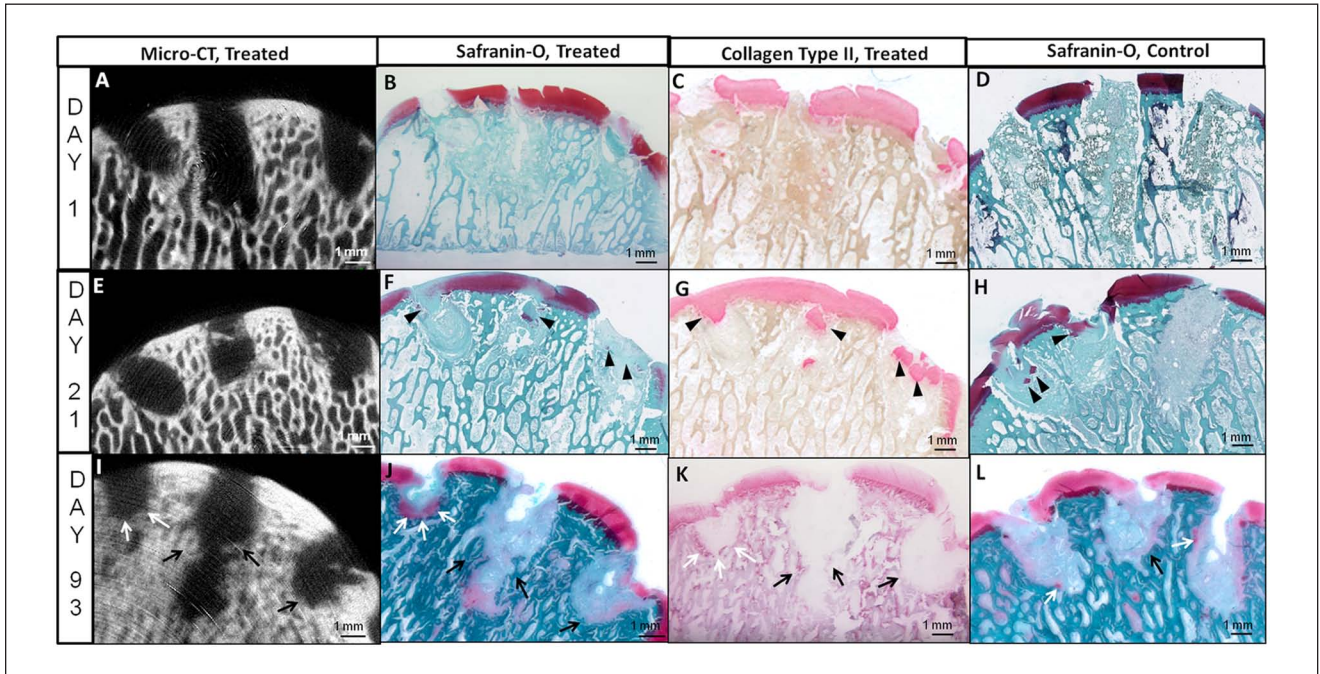


Figure 3. Micro-computed tomography images and corresponding Safranin O–stained and collagen type II–immunostained sections through chitosan-treated Jamshidi biopsy needle holes, and Safranin O images of matching contralateral controls in medial femoral condyles at day 1 (**A–D**), 3 weeks (**E–H**), and 3 months (**I–L**). Panels **B** to **D** and **F** to **H** were generated from cryosections and panels **J** to **L** from methylmethacrylate (MMA) sections. In treated condyles the left hole = 150 kDa chitosan, middle hole = 40 kDa chitosan, and right hole = 10 kDa chitosan. Evidence of bone remodeling and new bone growth (black arrows) as well as chondroinduction (white arrows) after 3 months is shown in panels **I** to **L**. Black arrowheads indicate articular cartilage fragments pushed into holes from adjacent cartilage.

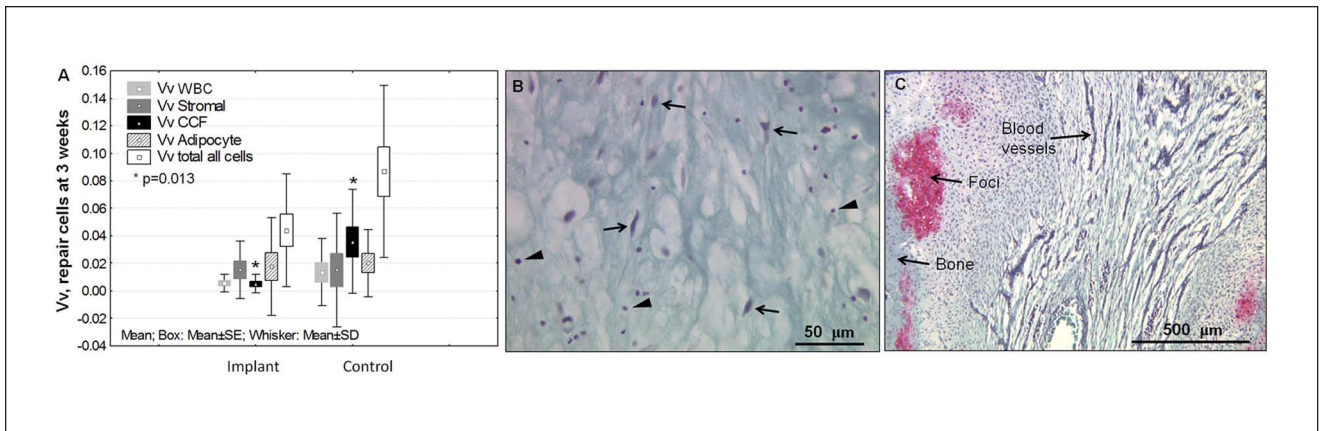


Figure 4. Soft tissue repair progression in Jamshidi holes from 3 weeks to 3 months consists in granulation tissue repair maturation, angiogenesis, and the induction of chondrogenic foci. **(A)** Quantitative unbiased stereology in the middle of the holes at 3 weeks showed the presence of leukocytes (white blood cells, WBC), stromal cells, chondrocytes in cartilage flow (CCF), and adipocytes, with significantly more cartilage flow present in controls ($P = 0.013$, $N = 12$ holes per condition). The average volume densities (Vv) with standard error boxes and standard deviation whiskers are shown. Hole depth (Table 2) and cartilage flow may have influenced recruitment of cells. Representative granulation tissue at 3 weeks in a Gomori-stained cryosection **(B)** shows sparse spindle-shaped stromal cells (arrows) and WBC (arrowheads), and a Safranin O–fast green stained cryosection at 3 months **(C)** shows mixed vascular granulation tissue and chondrogenic foci attached to remodeling bone (pink stain).

arrows, **Fig. 5A**). Some cartilage repair tissues over the holes had a large cleft (**Fig. 5A**), resulting in a mean integrity score of 1 for treated and untreated defects, on a scale of 0 (full-thickness defect, cleft) to 2 (smooth articular

surface). Jamshidi holes showed irregular borders and were filled with mainly vascular granulation tissue (**Figs. 3J–L** and **4C**). Most Jamshidi holes showed signs of chondroinduction, also termed chondrogenic foci (Chevrier *et al.*

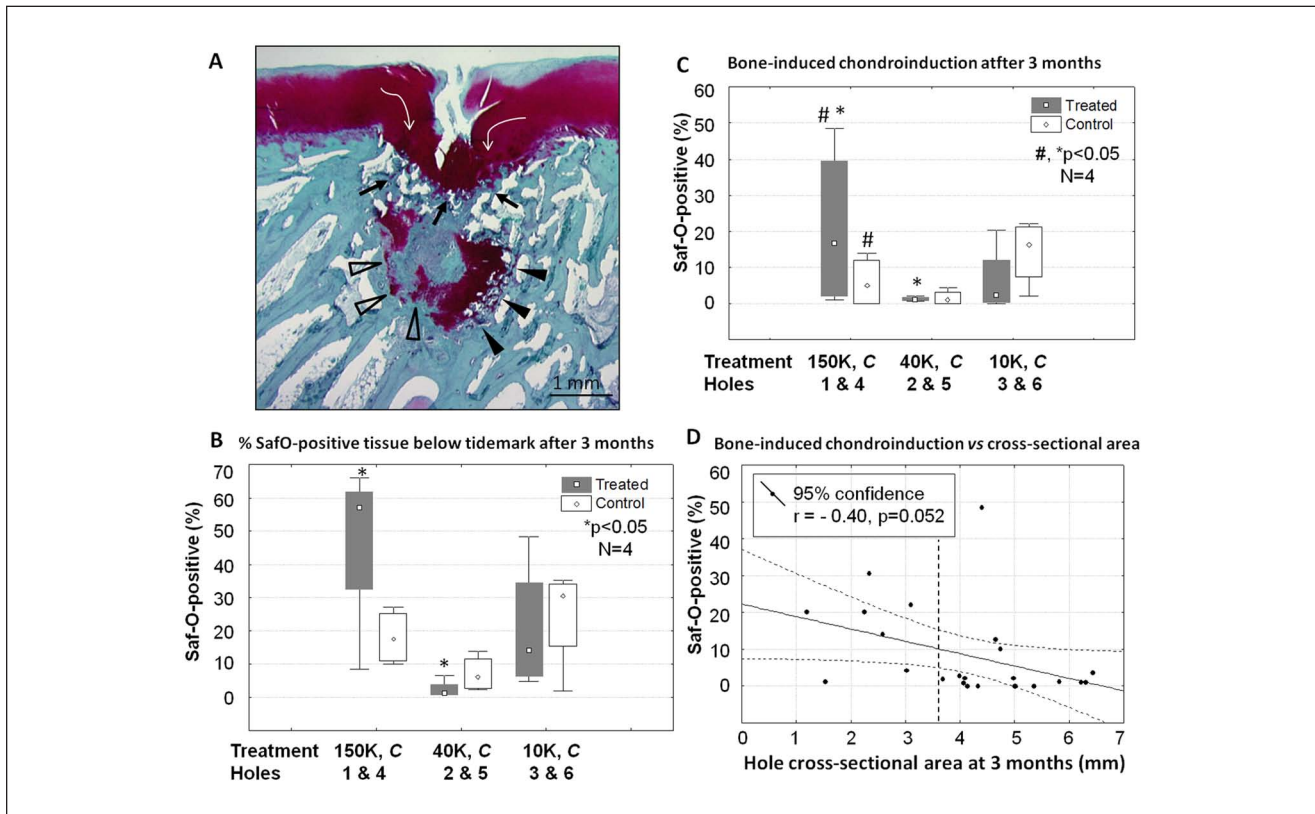


Figure 5. Subchondral new cartilage formation (chondroinduction) is variably present at the bone perimeter of Jamshidi defects at 3 months postoperative. Panel **A** shows a 150 kDa chitosan-treated Jamshidi defect at 3 months postoperative with cartilage flow (white arrows), bone-induced chondroinduction at the bone plate (black arrows), and trabecular bone-induced chondroinduction with “nascent” chondrogenic foci (open arrowheads), and “mature” chondrogenic foci containing hypertrophic chondrocytes and undergoing endochondral ossification at the cartilage-bone interface (black arrowheads). Histomorphometry at 3 months postoperative analyzed percentage Safranin O–positive subchondral repair tissues for the 3 chitosan treatments and the position-matched contralateral control holes ($N = 4$), including (**B**) total Safranin O–positive tissue below the tidemark (combined bone chondroinduction and cartilage flow) and (**C**) chondroinduction induced by bone. (**D**) Multiple correlation analysis of chondroinduction versus hole cross-sectional area at 3 months. Panels **B** and **C**: median (point), 25% to 75% range (box), 1% to 99% percentiles (whiskers). Symbols: **C**, control untreated Jamshidi holes in a matching position on the condyle; **D**, horizontal dashed line shows average initial defect cross-sectional area of 2.2 mm, $N = 12$); *,# $P < 0.05$ between conditions.

2011).¹² Foci were recognized as variably sized Safranin O–stained tissues lining the bone hole (Figs. 4C and 5A) or fused to the repairing bone plate (Fig. 6). At the top of the holes, chondroinduction was distinguished from cartilage flow by a more dense and disorganized cellularity inside the Safranin O–positive tissues (Fig. 6). More cartilage tissue was observed inside the lateral holes (150 kDa and 10 kDa treated) compared with the central load-bearing holes (Fig. 5B). The 150-kDa treatment elicited more bone-associated chondrogenic foci than position-matched untreated control Jamshidi holes, and also more than the 40-kDa treatment (17% vs. 1%, 150 kDa vs control vs 40 kDa, $P < 0.05$, $N = 4$, Fig. 5C). Bone-induced chondroinduction tended to correlate with narrowing hole cross-sectional area at 3 months ($P = 0.052$, $r = -0.40$, $N = 24$, Fig. 5D) but not to hole depth at surgery or at 3 months. These data suggested that bone

holes were repairing from the outside-in (as opposed to the bottom-up) through an endochondral mechanism.

μ CT Measures of Mineralized Bone Repair

μ CT measures at necropsy showed that bone hole depth and diameter were stable between 1 day and 3 weeks postoperative, after which holes became on average ~ 1 mm deeper with a more irregular hole diameter at 3 months, particularly for treated defects (Table 2). To analyze the irregular bone hole perimeter, a novel μ CT radial analysis was developed that quantified the average bone volume fraction and bone mineral density from the center of each hole radiating outward (Fig. 7A and B). An average linear curve was created for all treated versus all untreated holes at each time point ($N = 12$). A sharp slope at day 1 indicated the normal

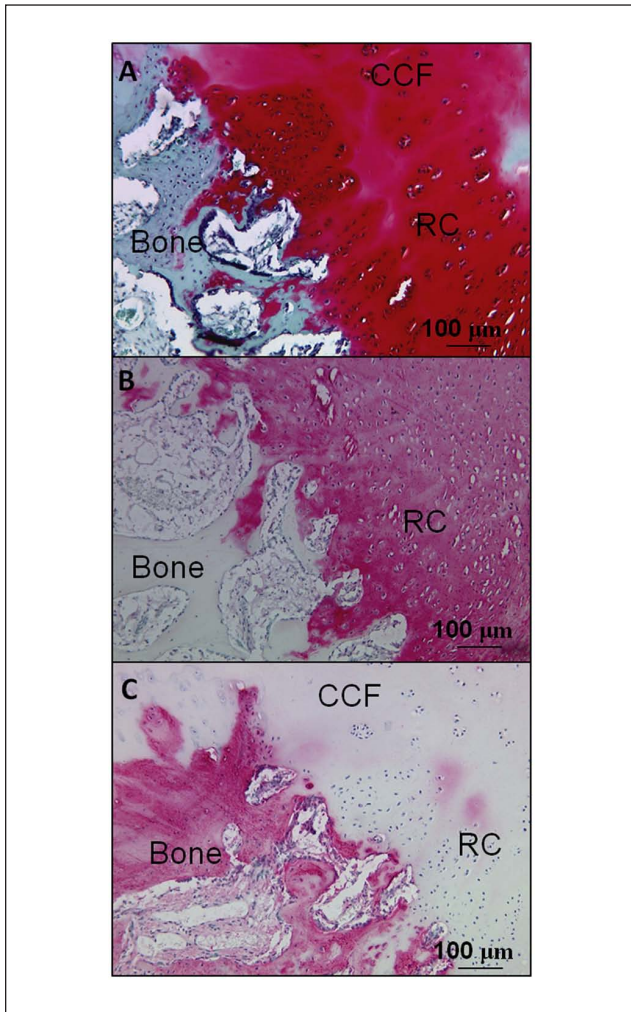


Figure 6. Bone plate–induced chondroinduction in serial sections from a 150 kDa treated defect at 3 months postoperative stained for Safranin O (**A**) or immunostained for collagen type II (**B**) or collagen type I (**C**). CCF = chondrocytes in cartilage flow; RC = repair cartilage.

transition between the cylindrical hole and surrounding bone (solid black line, **Fig. 7C** and **D**). At 3 weeks postoperative, there is little repair, but after 3 months there is a more gradual transitional slope in both control and treated defects that extends beyond the initial hole border, indicating both repair and remodeling ongoing at the repair tissue–bone interface (**Fig. 7C** and **D**). Remodeling refers to coupled osteoclast–osteoblast activity along bone surfaces, which can be readily observed by histology. In our μ CT analysis, remodeling is revealed by a diminished bone density outside the initial defect radius and volume increase inside the defect that reflects new mineralized tissue. A significantly higher bone volume fraction was observed inside treated versus untreated defects at 3 months ($P = 0.017$, $N = 12$).

Nondecalcified plastic histology generated in this study provided a unique opportunity to analyze mineralized tissue

in healing Jamshidi defects. At day 1, the Jamshidi hole edges were splintered (**Fig. 8A**) and cartilage flow fragments with attached calcified cartilage were also present in some holes (not shown). At 3 months postoperative, the bone splinters were replaced by a combination of new woven bone formation and areas of endochondral ossification (**Fig. 8**). Holes containing mature subchondral chondrogenic foci at the base showed punctate mineral inside cartilage that was contiguous with the adjacent trabecular bone mineral (white arrows, **Fig. 8C** and **D**). In some defects, the bone plate was repairing horizontally and closing the top of the Jamshidi hole with new cartilage repair tissue above and granulation tissue below (**Figs. 5A** and **6**). A total of 4 out of 12 Jamshidi holes, in both treated and control groups, showed signs of bone plate–induced chondroinduction, and all of these Jamshidi holes had an initial depth of ≤ 3.5 mm. Bone plate–induced chondroinduction was absent in Jamshidi defects with cartilage flow fragments pressed along the bone plate edge.

Discussion

This study reports the novel finding that Jamshidi defects repair spontaneously via trabecular bone–induced chondroinduction (bone repair via endochondral ossification) and bone plate–induced chondroinduction (articular cartilage repair, **Figs. 5** and **6**). These data provide new insights on the critical and coupled role of bone and cartilage repair following marrow stimulation which assists in the design and optimization of novel treatments.

This study demonstrated the feasibility of creating and retaining presolidified chitosan–blood implants in subchondral bone channels generated with a Jamshidi biopsy needle. The implants could be delivered in less than a minute, compared with up to 7 to 15 minutes wait time for in situ solidification of liquid chitosan–glycerol phosphate/blood mixtures in previous animal studies and BST–CarGel in the clinic.^{6,10} Presolidified chitosan/blood implants were readily delivered by passive capillary action to bone defects in any orientation (vertical, upside-down), which could facilitate arthroscopic delivery; although implants delivered in this manner resided in unpredictable regions in the hole. At later times, some Jamshidi holes were sealing off at the top by bone plate–induced chondroinduction above angiogenic granulation tissue (**Fig. 5**). These observations are consistent with other studies showing that marrow stimulation defects can become resurfaced with hyaline-like tissue and bone over tissue voids,²³ cysts,⁵ or residual implant that persists in the deeper trabecular bone.^{24–26} A fast-degrading subchondral biomaterial such as chitosan may favor deeper bone regeneration (**Fig. 7**) compared with other subchondral implants that take longer than 3 months to degrade.²⁴

Generation of 6 Jamshidi defects in the same condyle generates more subchondral bleeding, alters the distribution

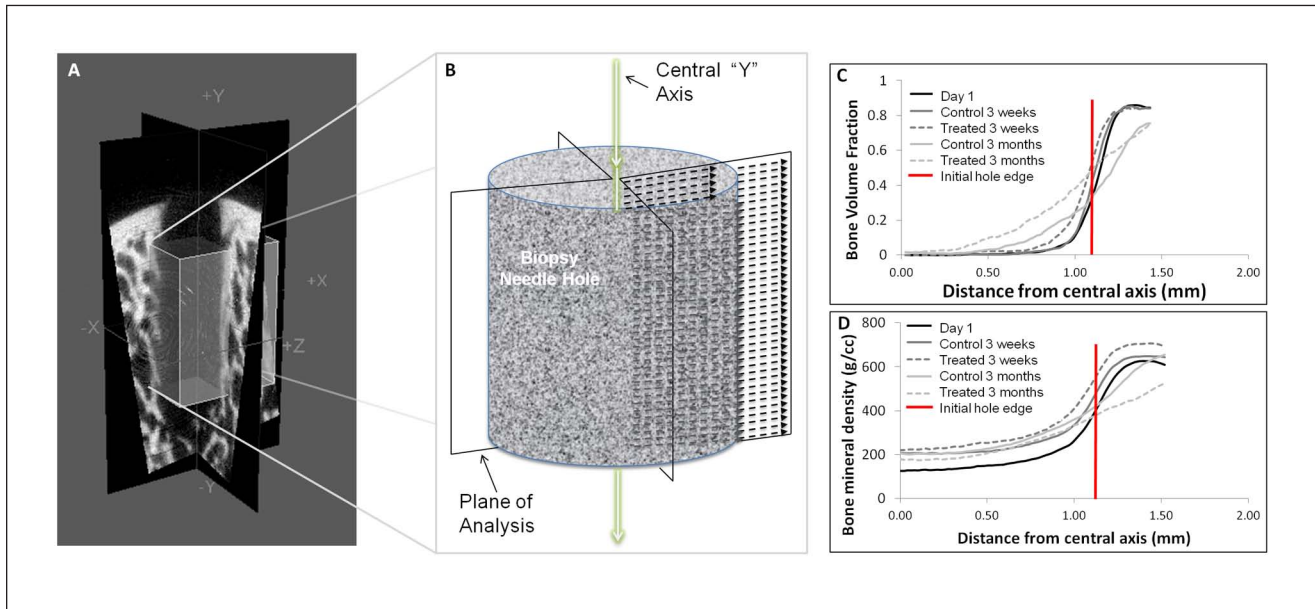


Figure 7. Depiction of micro-computed tomography (μ CT) radial analysis method and radial measures of bone volume fraction (BVF) and bone mineral density (BMD) changes in Jamshidi defects over time. **(A)** Two planes at 90° quadrisection the needle biopsy hole. Each μ CT slice is represented by the dashed arrows. **(B)** The 4 radial μ CT values from each 2-dimensional slice are averaged in the direction of the central “Y” axis. Radial analysis of holes for BVF **(C)** and BMD **(D)** was carried out on all day 1 holes ($N = 24$), and implant-treated ($N = 12$) and controls ($N = 12$) at 3 weeks and 3 months. The horizontal line shows the theoretical hole boundary for a 2.2-mm diameter hole (see **Table 2**). At 3 months postoperative, significantly more BVF was detected in treated versus control defects (using BVF values at 0.5, 0.75, and 1.0 mm from the center of the hole as repeated measures, $P = 0.017$, $N = 12$).

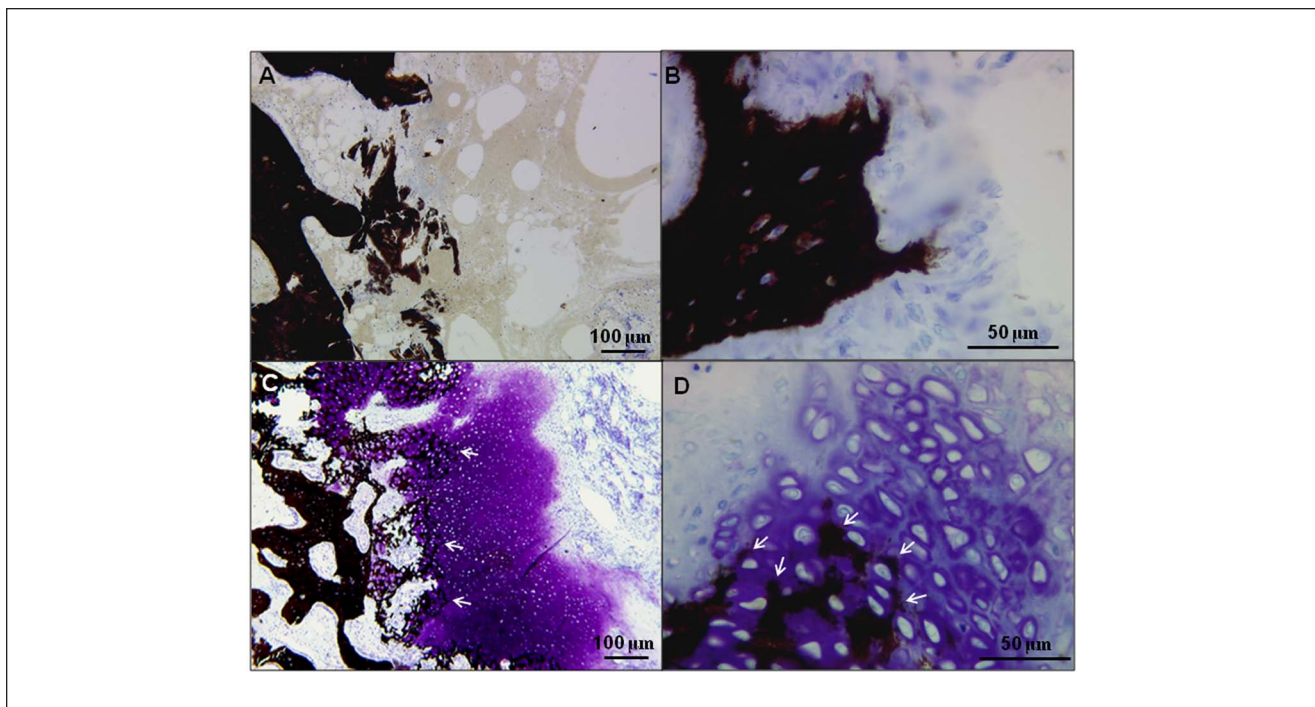


Figure 8. Initial Jamshidi needle bone defect edge and bone repair at 3 months postoperative at the repair tissue-bone interface below the bone plate. Nondecalfied plastic sections were stained with von Kossa (black stain for mineral phosphate) and toluidine blue (blue = protein, violet = glycosaminoglycan) from day 1 **(A)** and 3 months postoperative showing new woven bone **(B, treated defect)**, and endochondral ossification at the interface of mature chondrogenic foci and trabecular bone **(C and D, control defect)**. White arrows show mineral formation inside mature chondrogenic foci.

of forces, and may have influenced the repair response. Although in this study (Fig. 5A) and in previous work,²⁷ the repair response was well localized to the hole, suggesting that heterogeneity in the response can be detected on a site-by-site basis. The study was designed to screen 3 chitosan formulations for therapeutic effects but was underpowered. Small groups were used because this was a screening study of multiple formulations that investigated mechanism and proof of principle rather than being a pivotal fully powered study. Nonetheless, 150-kDa chitosan elicited more bone-induced chondroinduction compared with 40 kDa-treated holes and matching control defects, and treated holes showed more mineralized repair in-growth than controls. Mechanisms that elicit chondroinduction are still unclear, although current data show that “wound bloom” (incremental increase then closure of the wound)¹³ and angiogenesis (Figs. 4C and 6) can precede chondrogenic foci induction,^{8,9,11,12} while cartilage flow fragments pressed against the damaged bone blocked it. Biomaterial-induced vascular inflammation and bone remodeling should be further analyzed as a novel mechanism to guide cartilage formation from repairing bone surfaces.

Scarce information exists on repair progression of the defect generated by Jamshidi biopsy, which have been collected in a variety of clinical studies.^{2,4,28} In a horse cartilage repair model of microfracture, no apparent deleterious effects were observed at 12 months, from a biopsy taken at 4 months from the repair tissue in half of the defects.²⁹ In this study, Jamshidi biopsies led to osteoarthritic changes (osteophytes, fissuring) at 3 months postoperative, which was potentially related to the extensive subchondral bone damage and bruising from multiple biopsies (Fig. 1C and D).¹⁶ The cartilage fissuring seen in this study may be because biopsies were collected from normal articular cartilage instead of a repair site that is actively remodeling, which could be clinically relevant in noncompliant patients following mosaic arthroplasty, where multiple trephine biopsies are collected with a similar diameter as the Jamshidi needle.³⁰ Presolidified chitosan-blood implants show promise as an adjunct treatment to alleviate donor site morbidity following mosaic arthroplasty.

Striking differences in osteochondral defect repair progression were noted in sheep compared to rabbit. Sheep osteochondral Jamshidi defects were variably covered by cartilage flow (nonexistent in rabbits with thin ~120 μ m articular cartilage), which could impede cell recruitment from the synovial fluid. Sheep bone defects showed relatively weak stromal cell chemotaxis at 3 weeks (V_V ~2% vs ~12% in rabbit),⁸ delayed vascular granulation tissue formation and chondroinduction (~3 months vs ~3 weeks onset in rabbit),³¹ and negligible bone repair compared with a robust woven bone synthesis seen in rabbit drill holes after 2 to 3 months.^{9,31} Sheep osteochondral holes repaired from the “outside-in” in contrast to rabbit drill holes that repair from

the “bottom-up.”^{9,32} In a rabbit model, presolidified 10-kDa chitosan-blood implant press-fit into an osteochondral drill hole elicited a strong leukocyte and stromal cell chemotaxis at 3 weeks and reproducible bone plate-associated chondroinduction at 2.5 months.^{32,33} We speculate that lower cell chemotaxis to treated sheep defects could be due to inadequate filling of the sheep Jamshidi holes with implant, so a dose-response study is warranted. These collective observations highlight the challenges of developing new cartilage therapies that require scale-up from small animal to large animal models prior to clinical testing.^{34,35} Scale-up needs to take into serious consideration a much longer repair period in large animals, different bone and cartilage tissue properties, the appropriate scaled-up implant dosage, and how to generate subchondral channels in a way that a therapeutic repair response is elicited.

Research efforts have yet to identify the optimal subchondral bone loss needed to reproducibly elicit a therapeutic marrow-derived repair response. It was recently reported that more chondroinduction occurs after creating 6-mm versus 2-mm deep drill holes in a rabbit model,³¹ suggesting that deep drilling could have therapeutic advantages. Although in middle-aged human patients, Insall³⁶ found that drilled sclerotic bone can fail to regenerate even 12 months postoperative. Deep drilling in sheep condyles (10-mm deep, using a 1-mm diameter K-wire) led to subchondral cysts,³⁷ and in this study Jamshidi holes deeper than 3.5 mm tended to get bigger over the course of 3 months, instead of repairing. Moreover, significant remodeling seen outside the initial hole boundary, along with modest bone repair after 3 months, could potentially weaken subchondral bone mechanical properties.^{37,38} To further optimize the augmented surgical marrow stimulation method, future studies will focus on highly chemotactic implants and a surgical approach that generates more precision in hole depth and minimizes bone loss.

Acknowledgments and Funding

Financial support was from the Natural Sciences and Engineering Research Council of Canada (NSERC, Grant No. STPGP 365025), the Fonds de la Recherche en Santé du Québec (FRSQ) Groupe de Recherche en Sciences et Technologies Biomédicales (GRSTB), and salary support from the NSERC Alexander Graham Bell Canada Graduate Scholarship (AB), BioSyntech/Piramal Healthcare (JS), and FRSQ Bourse de carrière Senior (CDH). Technical facility support from the Canadian Arthritis Network is acknowledged.

Declaration of Conflicting Interests

In the previous 2 years, JS was employed by Piramal Healthcare, and several authors have consulted for Piramal Healthcare (CDH), RTI, Merck Research and Eli Lilly (MBH) for projects unrelated to the present work. CDH, JS, and MBH filed a patent with some data arising from this study. None of the authors have received payments or promises of payment related to the present work.

References

1. Steadman JR, Rodkey WG, Singleton SB, Briggs KK. Microfracture technique for full-thickness chondral defects: technique and clinical results. *Oper Tech Orthop.* 1997;7(4):300-4.
2. Knutsen G, Engebretsen L, Ludvigsen TC, Drogset JO, Grontvedt T, Solheim E, *et al.* Autologous chondrocyte implantation compared with microfracture in the knee: a randomized trial. *J Bone Joint Surg Am.* 2004;86(3):455-64.
3. Gobbi A, Nunag P, Malinowski K. Treatment of full thickness chondral lesions of the knee with microfracture in a group of athletes. *Knee Surg Sports Traumatol Arthrosc.* 2005;13(3):213-21.
4. Saris DB, Vanlauwe J, Victor J, Haspl M, Bohnsack M, Fortems Y, *et al.* Characterized chondrocyte implantation results in better structural repair when treating symptomatic cartilage defects of the knee in a randomized controlled trial versus microfracture. *Am J Sports Med.* 2008;36(2):235-46.
5. Hoemann CD, Hurtig M, Rossomacha E, Sun J, Chevrier A, Shive MS, *et al.* Chitosan-glycerol phosphate/blood implants improve hyaline cartilage repair in ovine microfracture defects. *J Bone Joint Surg Am.* 2005;87(12):2671-86.
6. Shive MS, Hoemann CD, Restrepo A, Hurtig MB, Duval N, Ranger P, *et al.* BST-CarGel: in situ chondroinduction for cartilage repair. *Oper Tech Orthop.* 2006;16(4):271-8.
7. Onishi H, Machida Y. Biodegradation and distribution of water-soluble chitosan in mice. *Biomaterials.* 1999;20(2):175-82.
8. Chevrier A, Hoemann CD, Sun J, Buschmann MD. Chitosan-glycerol phosphate/blood implants increase cell recruitment, transient vascularization and subchondral bone remodeling in drilled cartilage defects. *Osteoarthritis Cartilage.* 2007;15(3):316-27.
9. Hoemann CD, Chen G, Marchand C, Sun J, Tran-Khanh N, Chevrier A, *et al.* Scaffold-guided subchondral bone repair: implication of neutrophils and alternatively activated arginase-1+ macrophages. *Am J Sports Med.* 2010;38(9):1845-56.
10. Marchand C, Rivard GE, Sun J, Hoemann CD. Solidification mechanisms of chitosan-glycerol phosphate/blood implant for articular cartilage repair. *Osteoarthritis Cartilage.* 2009;17(7):953-60.
11. Hoemann CD, Sun J, McKee MD, Chevrier A, Rossomacha E, Rivard GE, *et al.* Chitosan-glycerol phosphate/blood implants elicit hyaline cartilage repair integrated with porous subchondral bone in microdrilled rabbit defects. *Osteoarthritis Cartilage.* 2007;15(1):78-89.
12. Chevrier A, Hoemann CD, Sun J, Buschmann MD. Temporal and spatial modulation of chondrogenic foci in subchondral microdrill holes by chitosan-glycerol phosphate/blood implants. *Osteoarthritis Cartilage.* 2011;19(1):136-44.
13. Chen G, Sun J, Lascau-Coman V, Chevrier A, Marchand C, Hoemann CD. Acute osteoclast activity following subchondral drilling is promoted by chitosan and associated with improved cartilage tissue integration. *Cartilage.* 2011;2:173-85.
14. Gomoll A, Madry H, Knutsen G, van Dijk N, Seil R, Brittberg M, *et al.* The subchondral bone in articular cartilage repair: current problems in the surgical management. *Knee Surg Sports Traumatol Arthrosc.* 2010;18(4):434-47.
15. Mithoefer K, Williams RJ 3rd, Warren RF, Potter HG, Spock CR, Jones EC, *et al.* The microfracture technique for the treatment of articular cartilage lesions in the knee. A prospective cohort study. *J Bone Joint Surg Am.* 2005;87(9):1911-20.
16. Nakamae A, Engebretsen L, Bahr R, Krosshaug T, Ochi M. Natural history of bone bruises after acute knee injury: clinical outcome and histopathological findings. *Knee Surg Sports Traumatol Arthrosc.* 2006;14:1252-8.
17. Shirazi R, Shirazi-Adl A. Computational biomechanics of articular cartilage of human knee joint: effect of osteochondral defects. *J Biomech.* 2009;42:2458-65.
18. Brittberg M, Peterson L. Introduction of an articular cartilage classification. *ICRS Newslett.* 1998;8.
19. Peterson L, Minas T, Brittberg M, Nilsson A, Sjogren-Jansson E, Lindahl A. Two- to 9-year outcome after autologous chondrocyte transplantation of the knee. *Clin Orthop Relat Res.* 2000;(374):212-34.
20. Lavertu M, Methot S, Tran-Khanh N, Buschmann MD. High efficiency gene transfer using chitosan/DNA nanoparticles with specific combinations of molecular weight and degree of deacetylation. *Biomaterials.* 2006;27(27):4815-24.
21. Ma O, Lavertu M, Sun J, Nguyen S, Buschmann MD, Winnik FM, *et al.* Precise derivatization of structurally distinct chitosans with rhodamine B isothiocyanate. *Carbohydr Polymers.* 2008;72(4):616-24.
22. Ng HF. Automatic thresholding for defect detection. *Pattern Recogn Lett.* 2006;27(14):1644-9.
23. Marchand C, Chen G, Tran-Khanh N, Sun J, Chen H, Buschmann MD, *et al.* Microdrilled cartilage defects treated with thrombin-solidified chitosan/blood implant regenerate a more hyaline, stable, and structurally integrated osteochondral unit compared to drilled controls. *Tissue Eng Part A.* 2012;18(5-6):508-19.
24. Streitparth F, Schoettle P, Schlichting K, Schell H, Fischbach F, Denecke T, *et al.* Osteochondral defect repair after implantation of biodegradable scaffolds: indirect magnetic resonance arthrography and histopathologic correlation. *Acta Radiol.* 2009;50(7):765-74.
25. Xue D, Zheng Q, Zong C, Li Q, Li H, Qian S, *et al.* Osteochondral repair using porous poly(lactide-co-glycolide)/nano-hydroxyapatite hybrid scaffolds with undifferentiated mesenchymal stem cells in a rat model. *J Biomed Mater Res Part A.* 2010;94(1):259-70.
26. Kitamura N, Yasuda K, Ogawa M, Arakaki K, Kai S, Onodera S, *et al.* Induction of spontaneous hyaline cartilage regeneration using a double-network gel. *Am j Sports Med.* 2011;39(6):1160-9.
27. Kandel RA, Grynblas M, Pilliar R, Lee J, Wang J, Waldman S, *et al.* Repair of osteochondral defects with biphasic cartilage-calcium polyphosphate constructs in a sheep model. *Biomaterials.* 2006;27(22):4120-31.

28. Hoemann CD, Kandel R, Roberts S, Saris DBF, Creemers L, Mainil-Varlet P, *et al.* International Cartilage Repair Society (ICRS) recommended guidelines for histological endpoints for cartilage repair studies in animal models and clinical trials. *Cartilage*. 2011;2(2):153-72.
29. Frisbie DD, Morisset S, Ho CP, Rodkey WG, Steadman JR, McIlwraith CW. Effects of calcified cartilage on healing of chondral defects treated with microfracture in horses. *Am J Sports Med*. 2006;34(11):1824-31.
30. Hangody L, Kish G, Karpati Z, Szerb I, Udvarhelyi I. Arthroscopic autogenous osteochondral mosaicplasty for the treatment of femoral condylar articular defects. A preliminary report. *Knee Surg Sports Traumatol Arthrosc*. 1997;5(4):262-7.
31. Chen H, Hoemann CD, Sun J, Chevrier A, McKee MD, Shive MS, *et al.* Depth of subchondral perforation influences the outcome of bone marrow stimulation cartilage repair. *J Orthop Res*. 2011;29(8):1178-84.
32. Hoemann CD, Lafantaisie-Favreau C-H, Lascau-Coman V, Chen G, Guzman-Morales J. The cartilage-bone interface. *J Knee Surg*. 2012;25(2):85-98.
33. Lafantaisie-Favreau C, Guzmán-Morales J, Harris A, Smith TD, Sun J, Carli A, *et al.* Novel pre-solidified chitosan/blood implant provides local bone-marrow stimulation-associated biological activity in skeletally aged rabbits after a three week treatment. Presented at: International Cartilage Repair Society Congress; September 26-29, 2010; Barcelona, Spain.
34. US Food and Drug Administration. Guidance for industry: preparation of IDEs and INDs for products intended to repair or replace knee cartilage. In: Center for Biologics Evaluation and Research, editor. Rockville, MD: US Department of Health and Human Services, Food and Drug Administration; 2011. p. 1-20.
35. Hurtig MB, Buschmann MD, Fortier LA, Hoemann CD, Hunziker EB, Jurvelin JS, *et al.* Preclinical studies for cartilage repair: recommendations from the International Cartilage Repair Society. *Cartilage*. 2011;2(2):137-52.
36. Insall JN. Intra-articular surgery for degenerative arthritis of the knee. A report of the work of the late K. H. Pridie. *J Bone Joint Surg Br*. 1967;49(2):211-28.
37. Orth P, Goebel L, Wolfram U, Ong MF, Gräber S, Kohn D, *et al.* Effect of subchondral drilling on the microarchitecture of subchondral bone: analysis in a large animal model at 6 months. *Am J Sports Med*. 2012;40 (4):828-36.
38. Morgan EF, Mason ZD, Chien KB, Pfeiffer AJ, Barnes GL, Einhorn TA, *et al.* Micro-computed tomography assessment of fracture healing: relationships among callus structure, composition, and mechanical function. *Bone*. 2009;44(2):335-44.